A Journal of the Gesellschaft Deutscher Chemiker

Angewandte International Edition

GDCh

Chemie

www.angewandte.org

Accepted Article

Title: Tumor Triggered Disassembly of Multiple-Agent-Therapy Probe for Efficient Cellular Internalization

Authors: Juliang Yang, Jun Dai, Quan Wang, Yong Cheng, Jingjing Guo, Zujin Zhao, Yuning Hong, Xiaoding Lou, and Fan Xia

To be cited as: *Angew. Chem. Int. Ed.* 10.1002/anie.202009196

Link to VoR: https://doi.org/10.1002/anie.202009196

WILEY-VCH

10.1002/anie.202009196

WILEY-VCH

COMMUNICATION

Tumor Triggered Disassembly of Multiple-Agent-Therapy Probe for Efficient Cellular Internalization

Juliang Yang[+], Jun Dai[+], Quan Wang, Yong Cheng, Jingjing Guo, Zujin Zhao, Yuning Hong, Xiaoding Lou,* and Fan Xia

Abstract: Integration of multiple agent therapy (MAT) into one probe has been considered as a promising approach to improve therapeutic efficiency for cancer treatment. However, MAT probe, if entering the cell as a whole, might not be optimal for each individual therapeutic agent (with different physicochemical properties), to achieve their best performance, which hinders the strategy optimization. Here, we report a peptide-conjugated-AIEgen (FC-PyTPA): upon loading with siRNA, it can be self-assembled into FC_{siRNA}-PyTPA. When approaching the region near targeting tumor cells, FC_{siRNA}-PyTPA responds to extracellular MMP-2 and is cleaved into two parts: FC_{siRNA} and PyTPA. The former enters cells mainly by macropinocytosis and the latter is internalized into cells mainly through caveolae-mediated endocytosis. This dividing-into-two-part strategy greatly improves the internalization efficiency of each individual therapeutic agent. Once inside the cell, (1) self-assembly of nanofiber precursor F, (2) gene interference of C_{siRNA} and (3) ROS production of PyTPA are activated synergistically to successfully inhibit tumor growth.

Cancer that jeopardizes public health remains one of the most dreadful diseases. Owing to the complexity, diversity, and heterogeneity, numerous types of cancers cannot be eliminated completely.[1] Recently, by integrating of various therapeutic agents into one probe, multiple-agent-therapy probe (MATP), which could achieve maximized therapeutic efficiency with minimized side effects, has attracted huge research interests and been considered as a promising approach in cancer treatment.[2] Classical therapeutic agents include photosensitizers for photodynamic therapy (PDT), drugs for chemotherapy (CT), genes for gene therapy (GT) and so on. Through the diversified combinations, a number of MATPs have achieved remarkable antitumor effect.[3] Generally, in these "all-in-one" MATPs, different therapeutic agents co-transport into cells as a whole, subsequently realizing the corresponding therapeutic mechanisms.[4]

In fact, due to the distinctive physicochemical properties, large molecules or complexes are taken up via various endocytic pathways including macropinocytosis, clathrin-mediated endocytosis, caveolae-mediated endocytosis, as well as phagocytosis. For example, cationic cell penetrating peptides (CPPs) and their functionalized nanomaterials can be engulfed through the macropinocytosis pathway;[5] latex particles larger than 200 nm in diameter are internalized exclusively via a caveolae-dependent pathway, whereas smaller particles enter the cells by clathrin-mediated endocytosis;[6] phagocytosis involves the ingestion of large particles through phagosomes with the diameter over 250 nm.[7] Obviously, "all-in-one" MATPs with changeless structure cannot satisfy the optimal dominant pathway of each agent simultaneously to enter the cells efficiently, leading to the unfulfilled therapeutic effect.[8]

There is an urgent demand to develop a smart MATP that, when approaching tumor-cells, can be separated into several agents which then enter the tumor cells by their dominant pathway, respectively. In this proof-of-concept study, a tumor triggered disassembled MATP with unique cellular internalization capability for efficient cancer treatment was designed. We utilized aggregation-induced emission luminogens (AIEgens, generally show faint fluorescence in solutions but emit bright fluorescence in the aggregated state) [9], and constructed a peptide-conjugated-AIEgen (FC-PyTPA) loaded with siRNA. We demonstrated efficient cellular internalization of triple therapeutic agents (nanofiber precursor, siRNA and photosensitizer) through two dominant internalization pathways (macropinocytosis for FC_{siRNA}; caveolae-mediated endocytosis for PyTPA). As shown in Scheme 1 (upleft part), FC-PyTPA contains three segments. (1) An amphiphilic structure with 16-carbon alkyl chain and GGGH peptide segment (F, blue part of FC-PyTPA).[10] It could self-assemble to form nanofibers and kill cancer cells.[11] (2) A positively charged peptide, GRKKRRQRRR (C, black part of FC-PyTPA), which transports cell-impermeable therapeutic genes (siRNA) into cells through electrostatic interaction.[12] (3) An AIE-based photosensitizer (PyTPA, red part of FC-PyTPA), which is an azide-functionalized triphenylamine derivative for image-guided PDT. In addition, matrix metalloproteinase-2 (MMP-2) responsive peptide PLGLAG and cathepsin B (CB) responsive peptide GFLG are incorporated in this design and act as linkers in FC-PyTPA.[13] Then, FC-PyTPA was loaded with siRNA through electrostatic interactions.[14] When approaching the tumor-cells, FC_{siRNA}-PyTPA could be specifically cleaved into two parts in the presence of MMP-2, which is overexpressed in tumor microenvironment.[15] One part, FC_{siRNA} can enter cells mainly by means of macropinocytosis and be trapped in lysosomes. The other part PyTPA can be internalized simultaneously mainly through caveolae-mediated endocytosis.

[*] J. Yang, Q. Wang, Dr. Y.Cheng, Prof. X. Lou, Prof. F. Xia
Engineering Research Center of Nano-Geomaterials of Ministry of Education, Faculty of Materials Science and Chemistry, China University of Geosciences
Wuhan 430078, China
E-mail: louxiaoding@cug.edu.cn
Dr. J. Dai
Department of Obstetrics and Gynecology, Tongji Hospital, Tongji Medical College, Huazhong University of Science and Technology, Wuhan, 430030, China
J. Guo, Prof. Z. Zhao
State Key Laboratory of Luminescent Materials and Devices, Guangdong Provincial Key Laboratory of Luminescence from Molecular Aggregates, South China University of Technology, Guangzhou, 510640, China
Prof. Y. Hong
Department of Chemistry and Physics, La Trobe Institute for Molecul ar Science, La Trobe University,
Melbourne, VIC 3086, Australia
[+] These authors contributed equally to this work.
Supporting information for this article is available on the WWW under http://

10.1002/anie.202009196

WILEY-VCH

COMMUNICATION

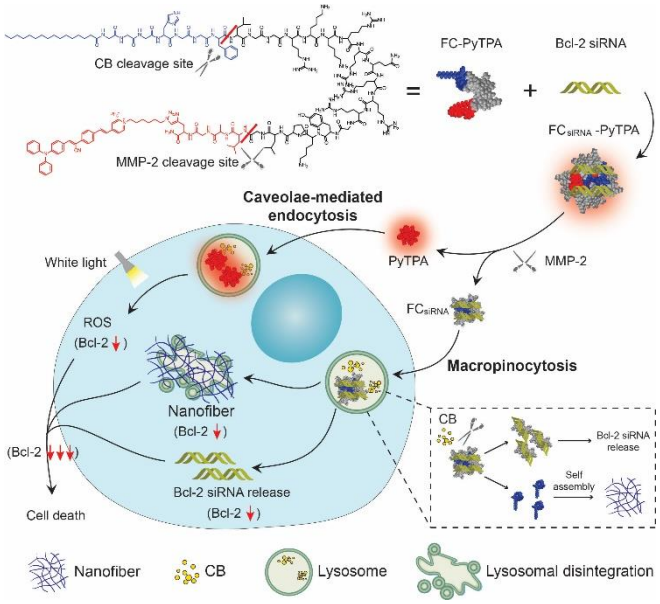

Scheme 1. FC-PyTPA and Bcl-2 siRNA are assembled into FC$_{siRNA}$-PyTPA complex, which can be divided into two parts (FC$_{siRNA}$ and PyTPA) once approaching tumor-cells with overexpressed MMP-2, which is secreted from tumor cells to the extracellular matrix. FC$_{siRNA}$ and PyTPA enter cells mainly through macropinocytosis and caveolae-mediated endocytosis pathway, respectively, and play multiple therapeutic functions.

Once FC$_{siRNA}$ enters into the cells, it can be hydrolyzed by CB to facilitate the formation of nanofibers via molecules self-assembly. The resulting nanofibers critically destroy the lysosomal structure and enable the escape of siRNA.[16] Under white light irradiation, the aggregation of PyTPA exhibited fluorescence image-guided PDT property. Consequntly, this smart MATP enables efficient internalization of triple therapeutic agents (nanofiber, siRNA and PyTPA) and thus successfully inhibits tumor growth, indicating great potential in translational nanomedicine.

To prove the function of different segments, both FC-PyTPA and its six control probes C-PyTPA (without nanofiber-forming segment), FC-PyTPA-M (without MMP-2 cleavage site), FC-PyTPA-C (without CB cleavage site), FC (without image-guided PDT segment), C (only siRNA-loading segment) and PyTPA (only image-guided PDT segment) were designed and synthesized (Figure 1a; Scheme S1-4; Table S1-2). All the products were confirmed by high performance liquid chromatography (HPLC), high resolution mass spectra (HRMS) or nuclear magnetic resonance spectra (NMR) (Figure S1-16). FC-PyTPA, FC-PyTPA-M, FC-PyTPA-C and C-PyTPA showed similar UV-vis absorption spectra as that of PyTPA. However, their fluorescence intensity was significantly reduced when PyTPA was modified with the hydrophilic peptides, owing to the AIE property (Figure S17-19). The capacity of FC-PyTPA on loading siRNA was evaluated by agarose gel electrophoresis.[17] With full consideration of loading capacity, particle size and zeta potential, 50:1 was selected as the optimal combination ratio with high stability toward serum (Figure 1b; Figure S20-23). Then we confirmed that the photosensitizing activity of probe was attributed to PyTPA and not altered by modifying the peptide (9,10-anthracenediyl-bis(methylene)dimalonic acid (ABDA) as ROS indicator) (Figure 1c; Figure S24-25). In the following, fluorescence intensity changes were used to demonstrate that different probes were cleaved by MMP-2 and CB (Figure 1d; Figure S26-29). Furthermore, the formation of nanofibers was clearly observed in both FC-PyTPA and FC$_{siRNA}$-PyTPA after hydrolysis with CB through transmission electron microscope (TEM) and dynamic light scattering (DLS) (Figure 1e, f; Figure S30-34). The enzymatic hydrolysis products were confirmed via HRMS analysis (Figure S35-37).

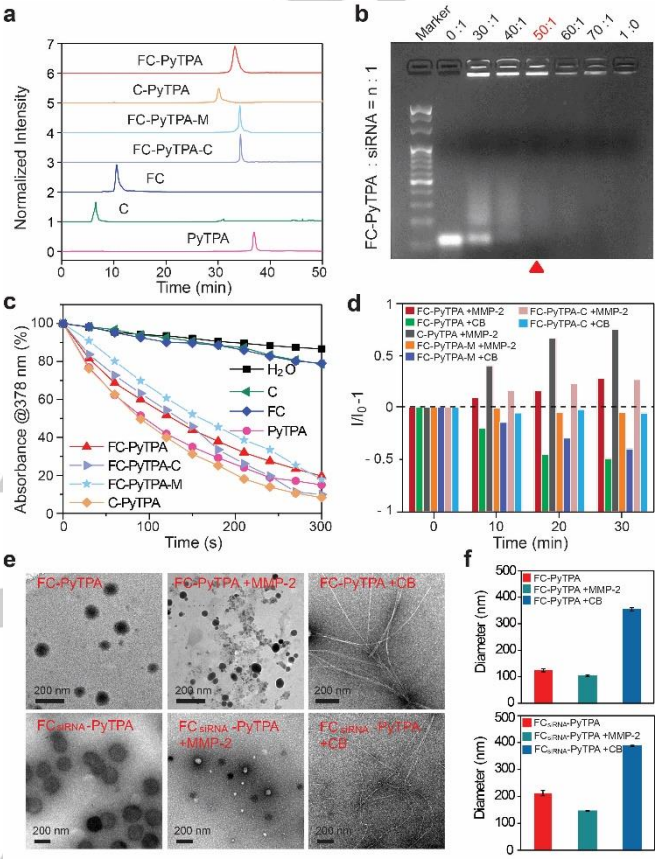

Figure 1. (a) HPLC spectra of different probes. (b) Agarose gel electrophoresis of the siRNA loading capacity of FC-PyTPA (50 μM). (c) Absorption spectra of the mixture containing ABDA (50 uM) and various probes (2.5 μM) upon white light irradiation (50 mW cm^{-2}) for different time. (d) Plot of I/I_0-1 versus different probes (2.5 μM) incubated with MMP-2 or CB (5.0 μg mL^{-1}) for 10, 20 and 30 min at 37 ^{0}C, respectively. (e) TEM images and (f) diameter distribution (DLS) of FC-PyTPA (5 μM) and FC$_{siRNA}$-PyTPA (5 μM) incubated with MMP-2 or CB (5.0 μg mL^{-1}).

In order to investigate the cellular internalization mechanism of FC$_{siRNA}$-PyTPA, three inhibitors EIPA (blocking macropinocytosis), CPZ (blocking clathrin-mediated endocytosis) and Filipin (blocking caveolae-mediated endocytosis) were utilized.[7] EIPA and Filipin showed the highest inhibition rate (I_0-$I_{inhibitor}$ /I_0) towards FC$_{siRNA\text{-}Cy5}$ (86%) and PyTPA (57%), respectively, when we physically mixed them, which was considered to achieve their own ideal cellular internalization efficacy (Figure 2a-b). The results indicated that macropinocytosis is the dominant pathway for FC$_{siRNA\text{-}Cy5}$, while PyTPA mainly enters cells through caveolae-mediated endocytosis. For our probe, as shown in Figure 2c-d, EIPA and Filipin inhibited most of FC$_{siRNA\text{-}cy5}$ and PyTPA, respectively, with inhibition rate of 75% and 50%, which is similar to the results in Figure 2a-b. We then investigated the role of MMP-2 in adjusting cellular uptake efficiency of FC$_{siRNA}$-PyTPA.

10.1002/anie.202009196

WILEY-VCH

COMMUNICATION

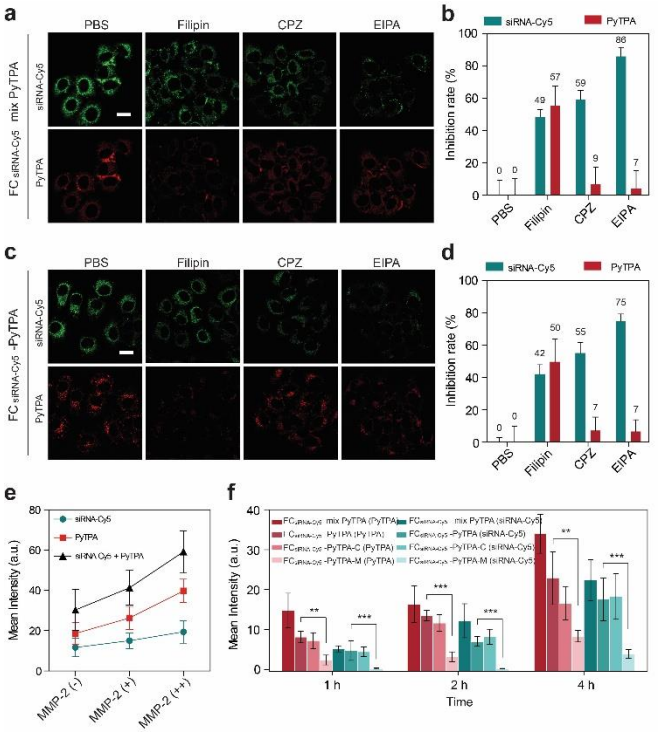

Figure 2. (a, c) Confocal laser scanning microscopy (CLSM) images and (b, d) the corresponding inhibition rate of HeLa cells treated with PBS (pH=7.4), Filipin (1 μg ml^{-1}), CPZ (10 μg ml^{-1}) or EIPA (10 μg ml^{-1}) for 30 min, then incubated with $FC_{siRNA\text{-}Cy5}$ mix PyTPA or $FC_{siRNA\text{-}Cy5}$-PyTPA (5 μM, 4 hours). (e) Mean fluorescence intensity of HeLa cells treated with $FC_{siRNA\text{-}Cy5}$-PyTPA (5 μM) for 4 hours. MMP-2 expression levels were regulated by washing cells with PBS. (f) Mean fluorescence intensity of HeLa cells incubated with $FC_{siRNA\text{-}Cy5}$ mix PyTPA, $FC_{siRNA\text{-}Cy5}$-PyTPA-M, $FC_{siRNA\text{-}Cy5}$-PyTPA-C or $FC_{siRNA\text{-}Cy5}$-PyTPA (5 μM) for 1, 2 and 4 hours. Green fluorescence (siRNA-Cy5, λ_{ex} =633 nm; λ_{em} =650–740 nm); red fluorescence (PyTPA, λ_{ex} =488 nm, λ_{em} =640–740 nm). Scale bars: 20 μm. Data are expressed as mean ± SD; $^{**}p < 0.01$, $^{***}p < 0.001$.

Since MMP-2 is mainly located in the extracellular matrix, expression levels of MMP-2 were regulated by washing cells with PBS and confirmed by enzyme-linked immunosorbent assay (ELISA) (Figure S38). The mean fluorescence intensity of siRNA-Cy5 and PyTPA increases significantly along with the MMP-2 expression levels and incubation time (Figure 2e; Figure S39-40). When incubating the probe with four cancer cell lines (MMP-2 expression level: SKOV3≈HeLa>PC3>MCF-7) (Figure S41) [18], the intracellular fluorescence intensity was positively correlated with MMP-2 expression level (Figure S42-48). In addition, statistical analysis was carried out for multiple comparisons (Figure 2f; Figure S49-50). With the incensement of incubation time, both the fluorescence of siRNA-Cy5 and PyTPA increased in $FC_{siRNA\text{-}Cy5}$ mix PyTPA, $FC_{siRNA\text{-}Cy5}$-PyTPA-M, $FC_{siRNA\text{-}Cy5}$-PyTPA-C or $FC_{siRNA\text{-}Cy5}$-PyTPA treated cells. The fluorescence in $FC_{siRNA\text{-}Cy5}$-PyTPA treated cells was comparable with that of $FC_{siRNA\text{-}Cy5}$-PyTPA-C, but higher than $FC_{siRNA\text{-}Cy5}$-PyTPA-M and lower than $FC_{siRNA\text{-}Cy5}$ mix PyTPA treated ones. Besides, the mean fluorescence intensity of HeLa cells incubated with siRNA-Cy5 was much lower than our probe (Figure S51). These results clearly demonstrated that MMP-2 played an important role in cleaving FC_{siRNA}-PyTPA and improving the cellular internalization efficiency of each segment.

In the following, we evaluated the effectiveness of each therapeutic agent after entering cells. The intracellular ROS

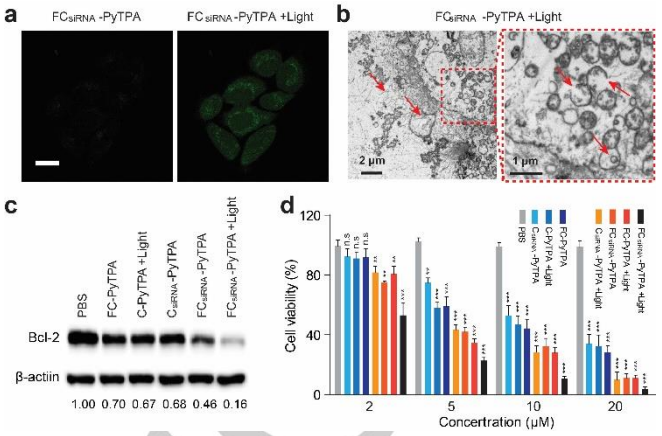

Figure 3. (a) CLSM images exhibit the intracellular ROS levels of FC_{siRNA}-PyTPA (5 μM) treated HeLa cells with DCFH-DA (10 μM, λ_{ex} =488 nm; λ_{em} =500–530 nm). White light irradiation (10 min; 200 mW cm^{-2}). Scale bar: 20 μm. (b) Bio-TEM images of HeLa cells after incubation with FC_{siRNA}-PyTPA (5 μM, 24 h). Red arrows indicate the nanofibers. Scale bar: 2 μm. (c) Western blotting analyses of the expressions of apoptosis-related protein Bcl-2 in HeLa cells under different treatments indicated. HeLa cells are incubated with FC_{siRNA}-PyTPA (5 μM, 24 h) and irradiated with white light (200 mW cm^{-2}, 10 min). (d) Cytotoxicities of HeLa cells upon different treatments by MTT assay. Data are expressed as mean ± SD; n.s.: no significant difference, $^{**}p < 0.01$, $^{***}p < 0.001$.

generating ability was studied using 2',7'-dichlorofluorescin diacetate (DCFH-DA) as an Intracellular ROS indicator. After white light irradiation, HeLa cells incubated with FC_{siRNA}-PyTPA, FC-PyTPA, C_{siRNA}-PyTPA or C-PyTPA exhibited bright green fluorescence, demonstrating that probes containing PyTPA can produce intracellular ROS (Figure 3a; Figure S52-54). Under the treatment of CB, FC_{siRNA}-PyTPA was converted into a nanofiber precursor confirmed by HRMS, which would then be able to self-assemble into nanofibers (Figure S55-56). Slender nanofibers were observed in lysosomes after the addition of FC_{siRNA}-PyTPA, while no nanofibers were observed in C_{siRNA}-PyTPA incubated cells (Figure 3b; Figure S57). It indicated that nanofibers could only be formed when 16-carbon alkyl chain "F" was present. We then photobleached the small area (white circle) staining by lysosomes indicator in Figure S58. The fluorescence did not recover 10 min after photobleaching. This result was attributed to the high viscosity inside lysosomes, implying the formation of nanofibers.[10c] The process of nanofibers-assisted lysosomal escape of siRNA was directly observed by CLSM and investigated using Lysotracker Blue as a lysosome indicator. The relative co-localization coefficient steadily decreased with extension of the incubation time (Figure S59). As illustrated in Figure S60, the PyTPA residue of FC-PyTPA mostly located in the lysosome. Figure S61 demonstrated that siRNA-Cy5 and PyTPA gradually separated with the increasing incubation time. Therefore, we could make a reasonable hypothesis that siRNA-Cy5 escaped from the lysosome. The Bcl-2 (apoptosis-related protein) expression level was confirmed by western blot assay (Figure 3c,). It was found that nanofiber therapy, photodynamic therapy and siRNA interference could down-regulate the expression of Bcl-2, but the effect was more effective when the three methods were combined. MTT assay revealed that probes at various concentrations had different cellular damage effects on HeLa cells and FC_{siRNA}-PyTPA +Light displayed the highest cytotoxicity (Figure 3d). These results demonstrated the effect of FC_{siRNA}-PyTPA in promoting cancer cell death.

10.1002/anie.202009196

Before the in vivo antitumor experiment, we first measured the time of FC_{siRNA}-PyTPA metabolism (Figure S62-63). HeLa tumor-bearing mice were randomly divided into 8 groups and received corresponding treatment. Tumor growth curves proved that FC_{siRNA}-PyTPA +Light group had significant tumor inhibition effect compared to other groups (Figure 4a). At the same time, during the treatment, there was almost no difference in the weight of the mice between the groups (Figure 4b). After treatment, tumors and organs were obtained for further examination. Bio-TEM showed that there were a lot of nanofibers in tumor tissues of FC_{siRNA}-

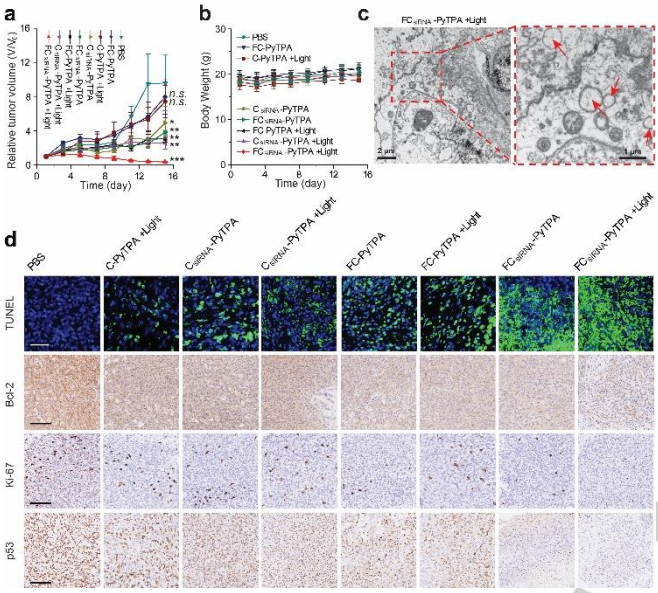

Figure 4. (a) Relative volume changes (V/V_0) and (b) body weight change of tumors in each group during treatment (n = 3). For the irradiation groups, the mice were exposed to white light (200 mW cm^{-2}) for 10 min. (c) Bio-TEM images of tumor slices of HeLa tumor-bearing mice model, after injection of FC_{siRNA}-PyTPA. Red arrows indicate the nanofibers. (d) TUNEL, Bcl-2, Ki-67 and p53 staining of HeLa tumor tissues after different treatments. Scale bar: 100 μm. Data are expressed as mean ± SD; n.s.: no significant difference, *$p < 0.05$, **$p < 0.01$, ***$p < 0.001$.

PyTPA +Light and FC_{siRNA}-PyTPA groups, but not in C_{siRNA}-PyTPA and PBS groups (Figure 4c and S64). Furthermore, TUNEL, Bcl-2, Ki67 and p53 staining results showed that FC_{siRNA}-PyTPA +Light group had the best anti-tumor effect than other groups (Figure 4d). In addition, H&E staining showed no obvious damage in the organs (Figure S65). Therefore, animal experimental results confirmed that the MATP based on peptide-modified-AIEgen is efficient for cancer treatment and has good biocompatibility.

In conclusion, we demonstrated a novel MATP (both extracellular MMP-2 and intracellular CB response) with high cellular internalization efficiency for effective multimodal cancer therapy. MATP divides into two parts, FC_{siRNA} and PyTPA, when approaching the region near targeting cells with relatively high concentration of MMP-2. The two parts then enter the cell in each's dominant pathway, which increases the total cellular internalization efficiency. The responsiveness of CB controls the lysosomal targeting and nanofibers formation of MATP. After hydrolysis of CB, the self-assembled nanofibers destroy the lysosomal structure and lead to the escape of siRNA for further gene silencing. Both in vitro and in vivo experiments confirm that the formation of nanofibers, the escape of siRNA and the ROS production of PyTPA effectively inhibit tumor growth. This study is also the first example of "all-in-one" MATP with enzyme response to divide into two-parts when approaching targeting cells with superior cellular internalization efficiency. The performance surpasses the control probe which enters the cell as an intact one. Our approach could inspire further investigation and provide insights in both the fields of nanotechnology and modular probe design.

Acknowledgements

This work is supported by the National Natural Science Foundation of China (21788102, 21722507, 21525523, 21974128, 21874121), the Natural Science Foundation of Hubei Province (2019CFA043) and Australian Research Council DE170100058.

Conflict of interest

The authors declare no conflict of interest.

Keywords: multiple-agent-therapy probe • peptide-conjugated-AIEgen • nanofibers/gene/ROS • macropinocytosis • caveolae-mediated endocytosis

[1] a) I. Dagogo-Jack, A. T. Shaw, *Nat. Rev. Clin. Oncol.* **2018**, *15*, 81-94; b) N. McGranahan, C. Swanton, *Cell* **2017**, *168*, 613-628; c) A. S. Cleary, T. L. Leonard, S. A. Gestl, E. J. Gunther, *Nature* **2014**, *508*,113-117.

[2] W. Fan, B. Yung, P. Huang, X. Chen, *Chem. Rev.* **2017**, *117*, 13566-13638.

[3] a) Z. Wang, Y. Ju, Z. Ali, H. Yin, F. Sheng, J. Lin, B. Wang, Y. Hou, *Nat. Commun.* **2019**, *10*, 4418; b) Y. Zhang, S. Bo, T. Feng, X. Qin, Y. Wan, S. Jiang, C. Li, J. Lin, T. Wang, X. Zhou, Z. Jiang, P. Huang, *Adv. Mater.* **2019**, *31*, 1806444; c) X. Zhang, Z. Xi, J. O. Machuki, J. Luo, D. Yang, J. Li, W. Cai, Y. Yang, L. Zhang, J. Tian, K. Guo, Y. Yu, F. Gao, *ACS Nano* **2019**, *13*, 5306-5325; d) M. Shevtsov, S. Stangl, B. Nikolaev, L. Yakovleva, Y. Marchenko, R. Tagaeva, W. Sievert, E. Pitkin, A. Mazur, P. Tolstoy, O. Galibin, V. Ryzhov, K. Steiger, O. Smirnov, W. Khachatryan, K. Chester, G. Multhoff, *Small* **2019**, *15*, 1900205; e) X. Yi, J. Dai, Y. Han, M. Xu, X. Zhang, S. Zhen, Z. Zhao, X. Lou, F. Xia, *Commun. Biol.* **2018**, *1*, 202; f) Y. Wang, G. Wei, X. Zhang, F. Xu, X. Xiong, S. Zhou, *Adv. Mater.* **2017**, *29*, 1605357; g) X. Tan, S. Luo, L. Long, Y. Wang, D. Wang, S. Fang, Q. Ouyang, Y. Su, T. Cheng, C. Shi, *Adv. Mater.* **2017**, *29*, 1704196; h) S. Tseng, Z. Liao, S. Kao, Y. Zeng, K. Huang, H. Li, C. Yang, Y. Deng, C. Huang, S. Yang, P. Yang, I. M. Kempson, *Nat. Commun.* **2015**, *6*, 6456.

[4] a) Kenry, K. C. Chong, B. Liu, *Acc. Chem. Res.* **2019**, *52*, 3051-3063; b) J. Qi, J. Li, R. Liu, Q. Li, H. Zhang, J. Lam, R. Kwok, D. Liu, D. Ding, B. Tang, *Chem* **2019**, *5*, 2657-2677; c) S. Wang, G. Yu, Z. Wang, O. Jacobson, L. Lin, W. Yang, H. Deng, Z. He, Y. Liu, Z. Chen, X. Chen, *Angew. Chem. Int. Ed.* **2019**, *58*, 14758-14763; *Angew. Chem.* **2019**, *131*, 14900-14905; d) S. Huo, N. Gong, Y. Jiang, F. Chen, H. Guo, Y. Gan, Z. Wang, A. Herrmann, X. Liang, *Sci. Adv.* **2019**, *5*, eaaw6264; e) J. Bai, X. Jia, W. Zhen, W. Cheng, X. Jiang, *J. Am. Chem. Soc.* **2018**, *140*, 106-109.

[5] a) Y. Wei, T. Tang, H. Pang, *Nat. Commun.* **2019**, *10*, 3646; b) H. Pang, G. B. Braun, E. Ruoslahti, *Sci. Adv.* **2015**, *1*, e1500821; c) H. Pang, G. B. Braun, T. Friman, P. Aza-Blanc, M. E. Ruidiaz, K. N. Sugahara, T. Teesalu, E. Ruoslahti, *Nat. Commun.* **2014**, *5*, 4904; d) L. Alberici, L. Roth, K. N. Sugahara, L. Agemy, V. R. Kotamraju, T. Teesalu, C. Bordignon, C. Traversari, G. Rizzardi, E. Ruoslahti, *Cancer Res.* **2013**, *73*, 804-812.

[6] J. Rejman, V. Oberle, I. S. Zuhorn, D. Hoekstra, *Biochem. J.* **2004**, *377*,159-169.

[7] M. A. Islam, Y. Xu, W. Tao, J. M. Ubellacker, M. Lim, D. Aum, G. Y. Lee, K. Zhou, H. Zope, M. Yu, W. Cao, J. T. Oswald, M. Dinarvand, M. Mahmoudi, R. Langer, P. W. Kantoff, O. C. Farokhzad, B. R. Zetter, J. Shi, *Nat. Biomed. Eng.* **2018**, *2*, 850-864.

[8] a) Y. Lu, A. A. Aimetti, R. Langer, Z. Gu, *Nat. Rev. Mater.* **2017**, *2*, 16075; b) M. P. Stewart, A. Sharei, X. Ding, G. Sahay, R. Langer, K. F. Jensen, *Nature* **2016**, *538*, 183-192; c) A. Panariti, G. Miserocchi, I. Rivolta, *Nanotechnol. Sci. Appl.* **2012**, *5*, 87-100.

[9] a) M. Gao, B. Tang, *Coord. Chem. Rev.* **2020**, *402,* 213076; b) G. Qi, F. Hu, Kenry, L. Shi, M. Wu, B. Liu, *Angew. Chem. Int. Ed.* **2019**, *58*,16229-16235; *Angew. Chem.* **2019**, *131*, 16375-16381; c) F. Hu, G. Qi, Kenry, D. Mao, S. Zhou, M. Wu, W. Wu, B. Liu, *Angew. Chem. Int. Ed.* **2020**, *59*, 9288-9292; *Angew. Chem.* **2020**, *132*, 9374-7378; d) C. Chen, H. Ou, R. Liu, D. Ding, *Adv. Mater.* **2019**, *31*, 1806331; e) C. Chen, X. Ni, S. Jia, Y. Liang, X. Wu, D. Kong, D. Ding, *Adv. Mater.* **2019**, *31*, 1904914; f) X. Ni, X. Zhang, X. Duan, H. Zheng, X. Xue, D. Ding, *Nano Lett.* **2019**, *19*, 318-330.

[10] a) H. Zhu, H. Wang, B. Shi, L. Shangguan, W. Tong, G. Yu, Z. Mao, F. Huang, *Nat. Commun.* **2019**, *10*, 2412; c) C. Zhang, L. Liu ,W. Qiu, Y. Zhang, W. Song, L. Zhang, S. Wang, X. Zhang, *Small* **2018**, *14*, 1703321; c) A. Tanaka, Y. Fukuoka, Y. Morimoto, T. Honjo, D. Koda, M. Goto, T. Maruyama, *J. Am. Chem. Soc.* **2015**, *137*, 770-775.

[11] a) H. Wang, Z. Feng, B. Xu, *J. Am. Chem. Soc.* **2019**, *141*, 7271-7274; b) H. Wang, Z. Feng, B. Xu, *Angew. Chem. Int. Ed.* **2019**, *58*, 10423-10432; *Angew. Chem.* **2019**, *131*, 10532-10541; c) D. Cheng, D. Wang, Y. Gao, L. Wang, Z. Qiao, H. Wang, *J. Am. Chem. Soc.* **2019**, *141*, 4406-4411; d) X. Zhao, L. Li, Y. Zhao, H. An, Q. Cai, J. Lang, X. Han, B. Peng, Y. Fei, H. Liu, H. Qin, G. Nie, H. Wang, *Angew. Chem. Int. Ed.* **2019**, *58*, 15287-15294; *Angew. Chem.* **2019**, *131*, 15431-15438; e) J. Zhan, Y. Cai, S. He, L. Wang, Z. Yang, *Angew. Chem. Int. Ed.* **2018**, *57*, 1813-1816; *Angew. Chem.* **2018**, *130*, 1831-1834.

[12] a) Y. Cheng, C. Sun, R. Liu, J. Yang, J. Dai, T. Zhai, X. Lou, F. Xia, *Angew. Chem. Int. Ed.* **2019**, *58*, 5049-5053; *Angew. Chem.* **2019**, *131*, 5103-5107; b) I. W. Hamley, *Chem. Rev.* **2017**, *117*, 14015-14041; c) Y. Liu, H. Wang, K. Kamei, M. Yan, K. Chen, Q. Yuan, L. Shi, Y. Lu, H. Tseng, *Angew. Chem. Int. Ed.* **2011**, *50*, 3058-3062; *Angew. Chem.* **2011**, *123*, 3114-3118.

[13] a) Z. Peng, J. Kopeček, *J. Am. Chem. Soc.* **2015**, *137*, 6726-6729; b) Y. Yuan, C. Zhang, M. Gao, R. Zhang, B. Tang, B. Liu, *Angew. Chem. Int. Ed.* **2015**, *54*, 1780-1786; *Angew. Chem.* **2015**, *127*, 1800-1806; c) L. Zhu, P. Kate, V. P. Torchilin, *ACS Nano* **2012**, *6*, 3491-3498; d) T. Jiang, E. S. Olson, Q. T. Nguyen, M. Roy, P. A. Jennings, R. Y. Tsien, *Proc. Natl. Acad. Sci. USA* **2004**, *101*, 17867-17872.

[14] a) R. A. Petros, J. M. DeSimone, *Nat. Rev. Drug. Discov.* **2010**, *9*, 615-627; b) A. Nel, T. Xia, L. Mädler, N. Li, *Science* **2006**, *311*, 622-627.

[15] a) V. H. Trang, X. Zhang, R. C. Yumul, W. Zeng, I. J. Stone, S. W. Wo, M. M. Dominguez, J. H. Cochran, J. K. Simmons, M. C. Ryan, R. P. Lyon, P. D. Senter, M, R. Levengood, *Nat. Biotechnol.* **2019**, *37*, 761-765; b) F. Wang, D. Xu, H. Su, W. Zhang, X. Sun, M. K. Monroe, R. W. Chakroun, Z. Wang, W. Dai, R. Oh, H. Wang, Q. Fan, F. Wan, H. Cui, *Sci. Adv.* **2020**, *6*, eaaz8985; c) L. Zhu, T. Wang, F. Perche, A. Taigind, V. P. Torchilin, *Proc. Natl. Acad. Sci. USA* **2013**, *110*, 17047-17052; d) K. Kessenbrock, V. Plaks, Z. Werb, *cell* **2010**, *141*, 52-67.

[16] a) J. Li, K. Shi, Z. F. Sabet, W. Fu, H. Zhou, S. Xu, T. Liu, M. You, M. Cao, M. Xu, X. Cui, B. Hu, Y. Liu, C. Chen, *Sci. Adv.* **2019**, *5*, eaax0937; b) T. Endoh, T. Ohtsuki, *Adv. Drug Deliv. Rev.* **2009**, *61*, 704-709.

[17] a) L. Y. Peddada, O. B. Garbuzenko, D. I. Devore, T. Minko, C. M. Roth, *J. Control. Release* **2014**, *194*, 103-112; b) T. C. Chu, K. Y. Twu, A. D. Ellington, M. Levy, *Nucleic Acids Res.* **2006**, *34*, e73.

[18] a) B. Coste, B. Xiao, J. S. Santos, R. Syeda, J. Grandl, K. S. Spencer, S. E. Kim, M. Schmidt, J. Mathur, A. E. Dubin, M. Montal, A. Patapoutian, *Nature* **2012**, *483*,176-181; b) The CCLE (Cancer Cell Line Encyclopedia) can be found under https://portals.broadinstitute.org/ccle/about.html, **2020**.

10.1002/anie.202009196

WILEY-VCH

Entry for the Table of Contents (Please choose one layout)

Layout 1:

COMMUNICATION

A novel multiple-agent-therapy probe based on peptide-conjugated-AIEgen was developed with extracellular MMP-2 and intracellular CB response. When approaching tumor cells, it can be separated into different agents which then enter the tumor cells by their dominant pathway with high cellular internalization efficiency and effective multimodal cancer therapy.

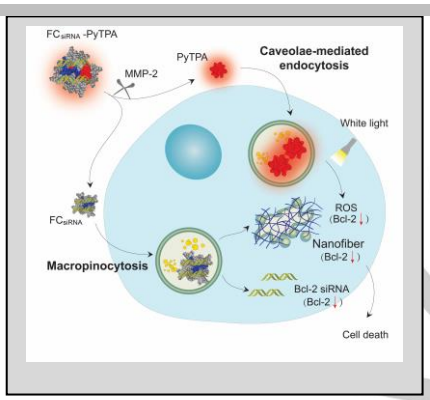

Juliang Yang+, Jun Dai+, Quan Wang, Yong Cheng, Jingjing Guo, Zujin Zhao, Yuning Hong, Xiaoding Lou, and Fan Xia*

Page No. – Page No.
Tumor Triggered Disassembly of Multiple-Agent-Therapy Probe for Efficient Cellular Internalization